Journal of Innovative Optical Health Sciences
Vol. 4, No. 3 (2011) 269–277

DOI: 10.1142/S179354581100154X

A DUAL-MODALITY OPTICAL BIOPSY APPROACH FOR *IN VIVO* DETECTION OF PROSTATE CANCER IN RAT MODEL

VIKRANT SHARMA*, NIMIT PATEL*, JINHUI SHEN,
LIPING TANG, GEORGE ALEXANDRAKIS and HANLI LIU†
Department of Bioengineering
Joint Graduate Program between University of Texas at Arlington
and University of Texas Southwestern Medical Center
University of Texas at Arlington, TX 76019, USA
†*hanli@uta.edu*

Accepted 25 April 2011

Ultrasound-guided biopsy procedure for prostate cancer diagnosis, which is the current gold standard, involves quasi-random sampling of prostate tissue without any functional guidance. In this study, we discuss the possibility to augment the detection of prostate cancer using a dual-modality optical approach, which can be coupled with the current needle biopsy setup. Two techniques are light reflectance spectroscopy (LRS) that uses a broadband light source and a CCD array spectrometer, and auto-fluorescence lifetime measurement (AFLM) that uses a custom-designed, time-correlated single photon counting (TCSPC) system. Both LRS and AFLM were employed sequentially in this study to measure cancer tissue along with control tissue on a rat prostate tumor model. At an excitation wavelength of 447 nm, we investigated auto-fluorescence decay curves at the emission wavelengths of 532, 562, 632 and 684 nm for *in vivo* and *ex vivo* AFLM. These results show that auto-fluorescence lifetimes at all measured emission wavelengths differ between control and cancerous tissues with 100% specificity and sensitivity. Moreover, absolute values of hemoglobin derivatives and scattering coefficient were quantified using *in vivo* LRS. This part of study also demonstrates that light scattering and absorption are significantly different between the control and cancerous tissue. Overall, the study demonstrates that both LRS and AFLM may provide several intrinsic biomarkers for *in vivo* detection of prostate cancer.

Keywords: Prostate cancer; light reflectance spectroscopy; auto-fluorescence lifetime.

1. Introduction

Prostate cancer is the most commonly found male cancer in the United States and is the second leading cause of death from cancer in men.[1] It was estimated that in 2009 that the number of new prostate cancer cases reported would be 192,280, resulting in 27,360 deaths.[2] At present, digital rectal examination (DRE), prostate specific antigen (PSA) blood test, and transrectal ultrasound (TRUS)-guided biopsy are the clinically available

*Both authors have contributed equally to this manuscript.
†Corresponding author.

techniques for prostate cancer screening and diagnosis. Among these, current gold standard for prostate cancer diagnosis is TRUS-guided needle biopsy, which involves resection of a core of prostate tissue with the guidance of an ultrasound probe. However, though ultrasound is able to provide high-resolution anatomical images, it lacks sensitivity in differentiating tumor from normal tissue, especially at early stages, making TRUS-guided biopsy a rather "blind" procedure involving quasi-random sampling of the prostate tissue.[3] This drawback leads to a high rate of false negative results and requires oversampling of tissue due to nonspecific targeting. The current standard biopsy procedure involves resection of 10−12 needle cores, and it was expected that by increasing the number of core biopsies, the accuracy in detecting cancer could be improved.[4] However, such an expectation is not proven by recent studies[5,6]; namely, saturation biopsy with 20−30 biopsy cores does not provide any significant improvement in correct diagnosis of prostate cancer. Moreover, increasing the number of cores often results in medical complications associated with the biopsy procedure.[4] It is, therefore, imperative to develop a targeting technique that can be used to guide the biopsy resection along the core so as to identify and collect highly suspicious prostate tissues on-site with high specificity and sensitivity.

In recent years, optical techniques have been popularly utilized to identify various cancers from their respective control tissues; many optical approaches have been implemented through needle probe geometry for minimally invasive procedures. Two specific techniques that can be implemented in such geometry are light reflectance spectroscopy (LRS) and auto-fluorescence lifetime measurement (AFLM). LRS has been used to characterize different types of tissues using either empirical or analytical methods.[7−13] Moreover, laser-induced steady-state auto-fluorescence spectroscopy and time-resolved lifetime measurement have been investigated for cancer detection.[14−20] While steady-state fluorescence measurements are easy to perform, they are intensity-dependent and hence sensitive to ambient light, excitation light intensity, measurement geometry, and probe setup. In contrast, temporally resolved fluorescence lifetime measurements are immune to all those interferences, only depending on specific fluorophores.

In this paper, we report the feasibility of both LRS and AFLM systems to be able to differentiate between cancerous and noncancerous tissues using a rat prostate cancer model with both *ex vivo* and *in vivo* measurements. LRS was used to calculate the absolute concentrations of oxy-hemoglobin, deoxy-hemoglobin and scattering properties of the tissue, while AFLM provided AFLM of the tissues by a single-channel, time-correlated single photon counting (TCSPC) device. After data analysis, we further tested the efficacy of using these multiple parameters as classifiers for identification of the tumor. The results presented in this paper provide us with the footprints for future *ex vivo* and *in vivo* measurements of human prostate cancer.

2. Animal Model and Preparation

A total of 4 one-year-old Copenhagen rats weighing 300−400 g were used in the study. Dunning R 3327 AT3.1 rat prostate carcinoma cells ($\sim 5 \times 10^6$) were injected subcutaneously on the foreback of each rat, followed by everyday monitoring of the tumor growth till it reached the volume of $\sim 1.5\,\text{cm}^3$. The rat was then anesthetized using a Ketamine/Xylazine combination. Once anesthetized, the rat had an incision made on the foreback to expose the tumor and a part of normal tissue. The exposed tissue/tumor surface was cleaned by flushing phosphate buffered saline (PBS), followed by multiple optical measurements with a bifurcated optical probe (see Fig. 1 and next subsection). All procedures for the animal studies were approved by IACUC at University of Texas at Arlington.

3. Auto-Fluorescence Lifetime Measurement

3.1. *Instrumentation for AFLM*

A custom-made, single-channel TCSPC (ISS Inc., Champaign, IL, USA) system was employed for AFLMs. Figure 1 on the right panel shows an overall experimental setup for the time domain AFLM. The system consists of a 12-V power supply unit, a stepper motor driving a five-slot filter wheel for excitation wavelength selection, a continuously variable neutral density (ND) filter for excitation light intensity control, an emission filter, and a highly sensitive cooled PMT (Becker & Hickl GmbH) with a wavelength range between 125−850 nm. The PMT gain was controlled via a PC-based interface board

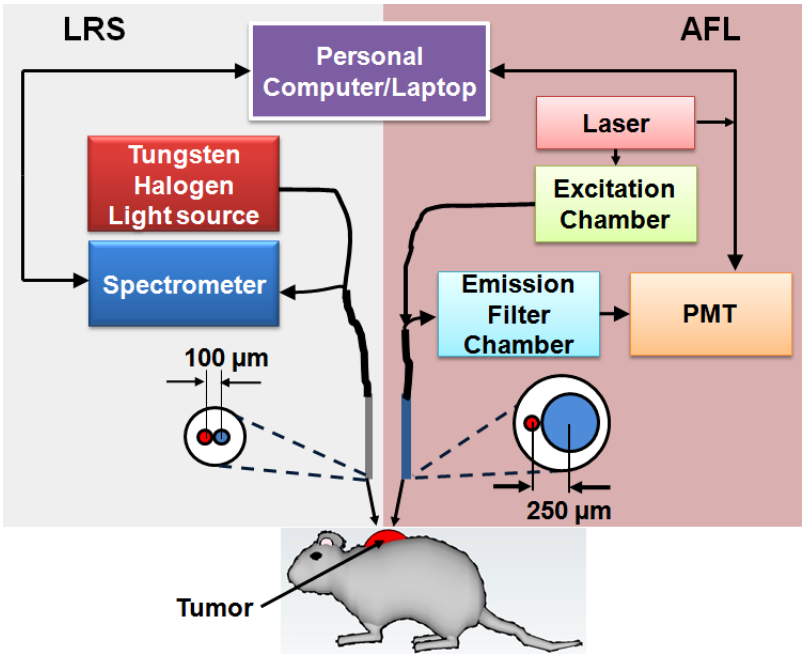

Fig. 1. A block diagram illustrating experimental setup for a LRS system (left) and AFL system (right). Measurements were made sequentially, by placing the fiber tips on the tissue surface. A closer view of bifurcated fiber tips are shown for each fiber (red = source; blue = detector).

(DCC-100). A broadband (400−1800 nm) pulsed laser (SC — 450, Fianium Inc., Eugene, Oregon, USA) with a pulse width of 5 ps was used as an excitation source at a repetition rate of 20 MHz. The exact synchronization between the laser pulse and the photon detection was achieved through a PC-based single photon counting card (SPC-130). The laser was coupled to the source fiber of the bifurcated optical probe with a core diameter of 100 μm; resulting fluorescence emission was collected through the detection fiber of a 400-μm core diameter from the other branch of the bifurcated probe.

3.2. *AFLM data analysis*

In this study, our auto-fluorescence signals result mainly from flavins, lipopigments and porphyrins that introduce optical contrasts to differentiate cancer from healthy tissue. In order to achieve maximum possible auto-fluorescence from all three endogenous compounds, an excitation wavelength of 447 nm was chosen.[16] While keeping the excitation wavelength constant, the emission wavelengths were changed among 532 nm, 562 nm, 632 nm and 684 nm. Filter selection and data collection was made through vender-provided software. The optical probe was placed at ∼1 mm away from the surface of the tissue. The *in vivo* fluorescence data were collected at five random positions from the exposed tumor and healthy tissue for each emission wavelength. By the end of the experiment, the animals were sacrificed, and the tumor and healthy tissue were extracted and kept in PBS for *ex vivo* measurements. Similar data collection procedure was also followed for *ex vivo* measurements. Thereafter, the detected fluorescence decay curves taken at all tissue positions were imported into Matlab (The Mathworks Inc., Natick, MA, USA) and normalized with respect to their peak intensities.

In order to quantitatively differentiate auto-fluorescence decay curves between cancer and control tissue, each curve was fitted by a least square nonlinear fitting algorithm, using a two-component exponential model:

$$\text{Intensity } (I) = \sum_i \alpha_i e^{-t/\tau_i}, \tag{1}$$

where, $\tau_i\,(i = 1, 2)$ indicates lifetime of each endogenous fluorophore; $\alpha_i\,(i = 1, 2)$ is the intensity contribution of each component to the overall fluorescence decay signal. The confidence interval on each of these four fitted parameters was computed using the "confint" function in Matlab. To count for both fluorophores with their respective weights, a

"mean lifetime", $\langle\tau\rangle$, was calculated using Eq. (2):

$$\langle\tau\rangle = \frac{\sum_i \alpha_i \times \tau_i^2}{\sum_i \alpha_i \times \tau_i}. \quad (2)$$

4. Light Reflectance Spectroscopy

4.1. *LRS instrumentation*

LRS system consists of a tungsten-halogen light source (HL2000HP, Ocean Optics, Dunedin, FL, USA), a CCD-linear-array spectrometer (USB 2000+, Ocean Optics, Dunedin, FL, USA), and a laptop computer. The spectrometer provided a spectrum ranging from 460−1150 nm. A custom-made, bifurcated fiber optic probe (Fiberguide Industries, Stirling, NJ, USA) was used, containing two of 100-μm core diameter fibers for both source and detector (s-d) with a s-d separation of ∼110 μm (Fig. 1). The probe was fixed on a stereotactic frame in order to steadily hold the probe in an accurate position and minimize the pressure on the tissue surface. Multiple data points were then obtained by placing the probe at different spatial locations on the tumor tissue and then the normal tissue. On an average, five data points were obtained from *in vivo* cancer and control tissue. Note that the *in vivo* LRS measurements were taken after *in vivo* AFLM readings. Since blood concentration and oxygenation state of hemoglobin in cancer tissue affect LRS greatly, no *ex vivo* measurement was taken with LRS due to severe alteration in hemodynamic environment from *in vivo* to *ex vivo* conditions.

4.2. *LRS data analysis*

Each acquired spectrum was divided by a reflectance spectrum obtained from a diffuse reflectance standard (WS-1, Ocean Optics, Dunedin, FL, USA) to eliminate spectral effects from the source, fibers, and detector. Then, the spectral range from 500−850 nm was selected; a reflectance model,[9] as shown in Eq. (1), was used to obtain absolute values of the concentrations of oxy-hemoglobin ([HbO]), deoxy-hemoglobin ([HbR]) and total hemoglobin ([HbT] = [HbR] + [HbO]), along with the reduced scattering coefficient (μ_s'),

$$R(\lambda) = \frac{\mu_s'(\lambda)}{k_1 + k_2 \cdot \mu_a(\lambda)}, \quad (3)$$

where R is the measured reflectance, $\mu_s'(\lambda)$ is the reduced scattering coefficient, μ_a is the absorption coefficient depending on the concentration of hemoglobin derivatives, and k_1 and k_2 are instrument-based parameters that depend only on the probe geometry and hardware setup. A detailed description of methodology to obtain the system-dependent parameters has been previously published.[21] Briefly, at first, k_1 and k_2 were calculated for the fiber optic probe using tissue-phantom calibration. Then, an optimization routine[22] (ant colony optimization) was used to fit the parameters of μ_s', [HbO], and [HbR], to optimally match the measured reflectance. The data processing was done using a code implemented in Matlab.

Because of a small s-d separation, the area of optical interrogation by this 200-μm probe is relatively small. It is possible that at certain locations, the probe can be on top of a large blood vessel, causing the reflectance signal to nearly diminish in 500−600 nm range due to high optical absorption of hemoglobin. Such spectra were identified and excluded as outliers in the data analysis. Overall, the dataset included five measurements in each tissue type (cancer and control) for rats 2 and 4, and four measurements each for rat 3. Also, data from rat 1 was obtained without the use of stereotactic frame, causing uncertainty in measurement location and pressure. Therefore, data from rat 1 was excluded from the analysis.

5. Results

The mean lifetime calculated at each emission wavelength was averaged over all four rats. Figures 2(a) and 2(b) show the comparison for averaged mean lifetime with standard deviation for *in vivo* and *ex vivo* measurements, respectively. It can be noticed from the plots that the averaged mean lifetime from cancer is lower than that from normal tissue in both cases at all emission wavelengths, as summarized in Table 1. This table also contains p-values that were obtained using a mixed model repeated measures ANOVA between the cancer and normal group. In addition, the average mean lifetime over four emission wavelengths were found to be 1.52 ± 0.09 ns and 2.61 ± 0.22 ns for *in vivo* cancer and control, respectively. As comparison, *ex vivo* measurements result in the averaged mean lifetime values of 2.82 ± 0.27 ns and 3.78 ± 0.31 ns for cancer and control, respectively. In order to see the effects of tissue degradation on mean lifetime, a mixed model repeated measures ANOVA

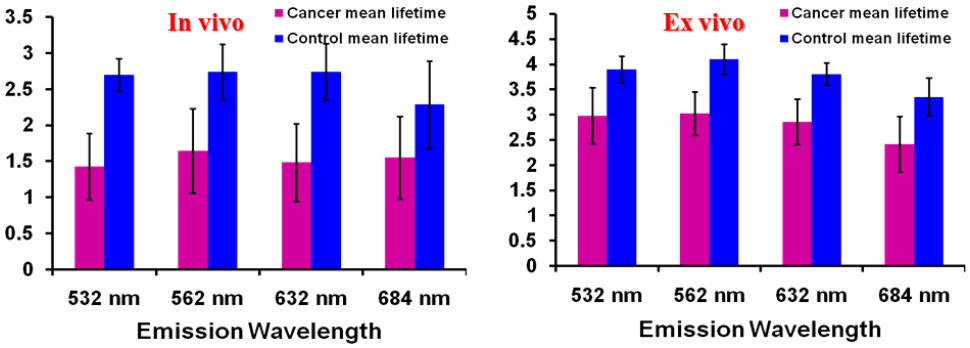

Fig. 2. Comparison of mean lifetime for (a) *in vivo* measurements, and (b) *ex vivo* measurements ($n = 20$).

Table 1. Summary for *in vivo* and *ex vivo* auto-fluorescence mean lifetimes.

		Emission wavelength (nm)			
		532	562	632	684
In vivo lifetime (ns)	Cancer	1.43	1.65	1.48	1.55
	Control	2.7	2.74	2.74	2.29
p-value		2.85×10^{-13}	5.70×10^{-8}	9.04×10^{-11}	2.0×10^{-4}
Ex vivo lifetime (ns)	Cancer	2.98	3.02	2.86	2.84
	Control	3.9	4.1	3.81	3.35
p-value		5.85×10^{-8}	3.54×10^{-9}	1.01×10^{-10}	4.87×10^{-7}

was performed between *in vivo* and *ex vivo* groups, revealing a significant difference between them.

Figure 3 shows the results of four parameters derived through LRS. The spectra were averaged over multiple points of each tissue type (either cancer or control) from each rat, and standard error of mean (SEM, represented by error bars) was calculated and shown. The values of [HbO] and [HbT] exhibit an increase in concentration in the tumor tissue as compared to the normal tissue in all three rats. The values of [HbR], on the other hand, were found to be very small compared to those of [HbO], and the standard error was relatively higher. Furthermore, the values of μ_s' were found to be smaller with a relatively small SEM in tumor tissue, as compared to those in the normal tissue. A mixed model ANOVA analysis for repeated measures revealed significant differences between tumor and

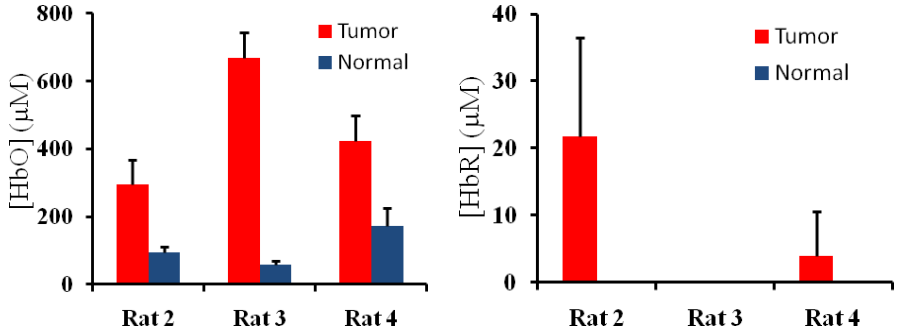

Fig. 3. Comparison of (a) [HbO], (b) [HbR], (c) [HbT], and (d) μ_s' values at 750 nm derived from *in vivo* rat tumor tissue and control tissue with LRS. Note that values of [HbR] are very heterogeneous, having a large range from 20 to 0.1 μM, some of which are unrecognizable in the figure.

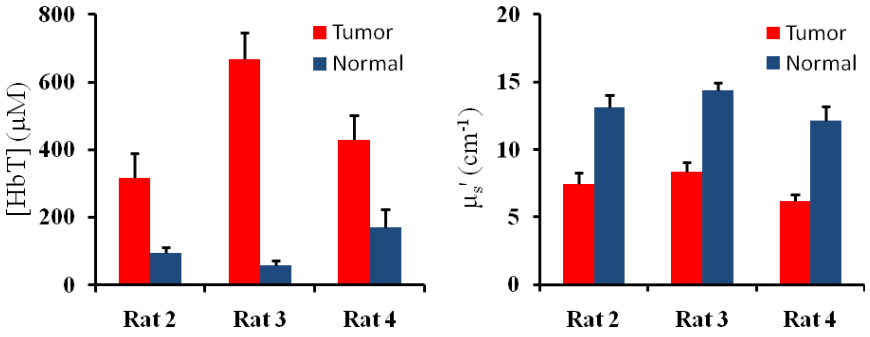

(c) (d)

Fig. 3. (*Continued*)

normal tissue in [HbO] ($p = 0.03$), [HbT] ($p = 0.03$), and μ_s' ($p = 0.01$). Difference in [Hb] was found to be insignificant with p-value of 0.22.

In order to evaluate whether any of the parameters hold potential to be used as an intrinsic biomarker, we employed support vector machine (SVM) as a classification algorithm.[23] In our approach, first, we chose any two independent parameters from the list of the fitted parameters, such as four mean lifetimes at the four emission wavelengths, [HbO], [HbT], and light scattering coefficient, as classifiers; second, we utilized the leave-one-out cross validation method to determine the sensitivity and specificity for the chosen paired classifiers. Since more than two parameters were available as classifiers, we used various combinations of parameters (see Table 2) to examine which pairs of parameters could be selected as best classifiers. For AFLM, with 20 data points available in each category (tumor and control) for testing, we obtained perfect sensitivity and specificity of 100% for all possible pairs in wavelength combinations. Table 2 lists only a couple of wavelength pairs as an example. If we considered the data from LRS, which had 14 data points available in each category, the best pair chosen as classifiers were determined to be [HbO] and μ_s' at 750 nm, which gave rise to both sensitivity and specificity of 92.86%.

6. Discussion and Conclusions

This study shows the feasibility of using LRS and AFLM as independent techniques for differentiating rat cancer tissue from normal tissue. Several optical parameters were obtained which could serve as potential biomarkers to identify cancerous tissue. Specifically, Figs. 2(a) and 2(b) present significant differences in mean lifetime between cancer and noncancerous tissue. Such results are expected since AFLM may be able to sense changes in temperature, pH, oxygen content, and nutrient supply of the measured tissue.[19–21] Because of such good sensitivity to local tissue environment, AFLM was found to be very robust, with 100% sensitivity and specificity when the mean lifetimes from any two wavelengths out of the four emission wavelengths were selected to classify cancer from normal tissue. Table 2 shows examples of two groups of wavelength combinations. The results also suggest

Table 2. Sensitivity and specificity values calculated for different pairs of obtained parameters using two modalities.

	Classification parameters				
	LRS ($n = 14$)			AFLM ($n = 20$)	
	[HbO] and [HbT]	μ_s' (750 nm) and μ_s' (830 nm)	[HbO] and μ_s' (750 nm)	532 nm and 562 nm	632 nm and 684 nm
Sensitivity (%)	71.43	78.57	92.86	100	100
Specificity (%)	71.43	92.86	92.86	100	100

difference in absolute lifetime values between *in vivo* and *ex vivo* measurements, while both cases exhibit a similar trend, namely, mean lifetime values were higher in normal tissues than those in cancerous tissues. This set of observations is also expected because rat tumor *ex vivo* samples may have experienced alternations in their physiological, metabolic, and biochemical condition, as compared to *in vivo* tissue, while being kept in PBS and measured ∼10 h after the extraction.

In case of LRS, an increase in total blood concentration was found; it is indicative of increased vasculature of tumor tissue (Fig. 3) as compared to normal tissue. It was also found that in most cases, [HbR] levels were very low, indicating a very high level of hemoglobin oxygen saturation (∼99%). This could be partially attributed to the fact that the optical readings were taken on the surface of the tissue which was exposed to room air. For deeper tumor regions, we may expect higher values of [HbR] as tumors are generally known to be hypoxic.[24] Furthermore, light scattering, which is closely associated with cell size and morphology, was found to be significantly different between tumor and normal tissues. This set of results is also expected as cell size and morphology are known to be different in cancerous cells compared to normal cells. It was further observed that μ_s' variability was relatively low at the individual level (indicated by error bars in Fig. 3), and that the μ_s' values were well significantly separated between the cancer and control groups, as indicated by a lower p-value of 0.01. To further increase the understanding of relation between μ_s' and cell morphology, and in turn to be used for cancer staging, we plan to include pathological analysis along with the optical quantification in our near-future studies.

While AFLM seems to be able to optimally determine or detect rat prostate cancer with perfect sensitivity and specificity, we are prepared to have a dual-modality approach to increase an improved detection power. This is because human prostate is quite different from a solid rat tumor and often has multifocal cancer lesions with different levels of cancer stage. It is highly possible that AFLM alone may not be able to clearly identify low-grade prostate cancer lesions, and a second detection modality, such as LRS, may provide a complementary solution.

To mimic real biopsy environments in the animal model, where the tissue is not directly exposed to room air and background auto-fluorescence may exist, a motorized system is planned to be implemented in order to drive the optical fiber into the tumor region in a minimally invasive manner with an appropriate step size. Also, use of orthotopic animal models of prostate cancer[25] can be an alternative option when investigating realistic tissue biopsy procedures. However, choosing an animal model that closely mimics the human prostate cancer could be challenging[26]; therefore, *ex vivo* measurements taken from human prostate specimens are necessary in order to validate our newly developed methodology.

In summary, we have found with a limited number of animals that both AFLM and LRS are robust methods to differentiate prostate tumor from normal tissue in rat prostate cancer model. It is seen that AFLM has high sensitivity and specificity and works well in both *in vivo* and *ex vivo* setups with comparable results (Fig. 2). However, AFLM is relatively costly; contact measurement geometry also needs to be explored. On the other hand, LRS is a much simpler system with effective cost. The sensitivity and specificity of this technique are relatively high, depending on which parameters are selected as classifiers. In near future, we plan to investigate the dual-modality approach in human prostate studies to develop and evaluate the classification abilities of the technique there. Although each individual technique (i.e., AFLM and LRS) or one of them may seem to be sufficient to differentiate cancer from noncancer, a combined approach in future may enhance our ability to detect and diagnose the tumor type (malignant or benign) and the stage of tumor.

Acknowledgments

This study was funded in part by Department of Defense (grant # W81XWH-09-1-0406) and Texas Ignition Fund.

References

1. A. Jemal, R. Siegel, E. Ward, Y. Hao, J. Xu, M. J. Thun, "Cancer statistics, 2009," *CA Cancer J. Clin.* **59**(4), 225−249 (2009).
2. American Cancer Society, "Cancer Facts and Figures 2009," Atlanta: American Cancer Society (2009).

3. N. B. Delongchamps, G. P. Haas, "Saturation biopsies for prostate cancer: Current uses and future prospects," *Nat. Rev. Urol.* **6**(12), 645−652 (2009).
4. U. Patel, "TRUS and prostate biopsy: Current status," *Prostate Cancer Prostatic Dis.* **7**(3), 208−210 (2004).
5. A. Descazeaud, M. Rubin, S. Chemama, S. Larre, L. Salomon, Y. Allory, D. Vordos, A. Hoznek, R. Yiou, D. Chopin, C. Abbou, A. de la Taille, "Saturation biopsy protocol enhances prediction of pT3 and surgical margin status on prostatectomy specimen," *World J. Urol.* **24**(6), 676−680 (2006).
6. J. S. Jones, A. Patel, L. Schoenfield, J. C. Rabets, C. D. Zippe, C. Magi-Galluzzi, "Saturation technique does not improve cancer detection as an initial prostate biopsy strategy," *J. Urol.* **175**(2), 485−488 (2006).
7. V. Sharma, D. Kashyap, A. Mathker, S. Narvenkar, K. Bensalah, W. Kabbani, A. Tuncel, J. A. Cadeddu, H. Liu, "Optical reflectance spectroscopy for detection of human prostate cancer," *Conf. Proc. IEEE Eng. Med. Biol. Soc.* **2009**, 118−121 (2009).
8. H. Liu, H. Radhakrishnan, A. K. Senapati, C. E. Hagains, D. Peswani, A. Mathker, Y. B. Peng, "Near infrared and visible spectroscopic measurements to detect changes in light scattering and hemoglobin oxygen saturation from rat spinal cord during peripheral stimulation," *Neuroimage* **40**(1), 217−227 (2008).
9. G. Zonios, A. Dimou, "Modeling diffuse reflectance from semi-infinite turbid media: Application to the study of skin optical properties," *Opt. Exp.* **14**(19), 8661−8674 (2006).
10. C. A. Giller, H. Liu, D. C. German, D. Kashyap, R. B. Dewey, "A stereotactic near-infrared probe for localization during functional neurosurgical procedures: Further experience," *J. Neurosurg.* **110**(2), 263−273 (2009).
11. M. Johns, C. Giller, D. German, H. Liu, "Determination of reduced scattering coefficient of biological tissue from a needle-like probe," *Opt. Exp.* **13**(13), 4828−4842 (2005).
12. K. Bensalah, D. Peswani, A. Tuncel, J. D. Raman, I. Zeltser, H. Liu, J. Cadeddu, "Optical reflectance spectroscopy to differentiate benign from malignant renal tumors at surgery," *Urology* **73**(1), 178−181 (2009).
13. S. C. Kanick, C. van der Leest, J. G. Aerts, H. C. Hoogsteden, S. Kascakova, H. J. Sterenborg, A. Amelink, "Integration of single-fiber reflectance spectroscopy into ultrasound-guided endoscopic lung cancer staging of mediastinal lymph nodes," *J. Biomed. Opt.* **15**(1), 017004 (2010).
14. F. Fischer, E. F. Dickson, J. C. Kennedy, R. H. Pottier, "An affordable, portable fluorescence imaging device for skin lesion detection using a dual wavelength approach for image contrast enhancement and aminolaevulinic acid-induced protoporphyrin IX. Part II. *In vivo* testing," *Lasers Med. Sci.* **16**(3), 207−212 (2001).
15. K. Izuishi, H. Tajiri, T. Fujii, N. Boku, A. Ohtsu, T. Ohnishi, M. Ryu, T. Kinoshita, S. Yoshida, "The histological basis of detection of adenoma and cancer in the colon by autofluorescence endoscopic imaging," *Endoscopy* **31**(7), 511−516 (1999).
16. G. A. Wagnieres, W. M. Star, B. C. Wilson, "*In vivo* fluorescence spectroscopy and imaging for oncological applications," *Photochem Photobiol.* **68**(5), 603−632 (1998).
17. J. Mizeret, T. Stepinac, M. Hansroul, A. Studzinski, H.v.d. Bergh, G. Wagnieres, "Instrumentation for real-time fluorescence lifetime imaging in endoscopy," *Review of Scientific Instruments* **70**(12), 4689−4701 (1999).
18. K. M. Katika, L. Pilon, K. Dipple, S. Levin, J. Blackwell, H. Berberoglu, "*In vivo* time-resolved autofluorescence measurements on human skin," *Proc. SPIE* **6078**, 60780L (2006).
19. M. A. Mycek, K. T. Schomacker, N. S. Nishioka, "Colonic polyp differentiation using time-resolved autofluorescence spectroscopy," *Gastrointest. Endosc.* **48**(4), 390−394 (1998).
20. N. Ramanujam, M. F. Mitchell, A. Mahadevan-Jansen, S. L. Thomsen, G. Staerkel, A. Malpica, T. Wright, N. Atkinson, R. Richards-Kortum, "Cervical precancer detection using a multivariate statistical algorithm based on laser-induced fluorescence spectra at multiple excitation wavelengths," *Photochem. Photobiol.* **64**(4), 720−735 (1996).
21. V. Sharma, J. W. He, S. Narvenkar, Y. B. Peng, H. Liu, "Quantification of light reflectance spectroscopy and its application: Determination of hemodynamics on the rat spinal cord and brain induced by electrical stimulation," *Neuroimage* **56**(3), 1316−1328 (2011).
22. D. Kashyap, "Development of a broadband multichannel NIRS system for quantifying absolute concentrations of hemoglobin derivatives and reduced scattering coefficients," Thesis Dissertation (2007).
23. S. R. Gunn, "Support vector machines for classification and regression," Image Speech and Intelligent Systems Research Group, University of Southampton (1997).
24. P. Vaupel, A. Mayer, "Hypoxia in cancer: Significance and impact on clinical outcome," *Cancer Metastasis Rev.* **26**(2), 225−239 (2007).

25. A. A. Alagbala, B. A. Foster, "Animal models of prostate cancer," in *Sourcebook of Models for Biomedical Research*, P. M. Conn, Ed., Humana Press, Inc., pp. 639−649, 2008.
26. K. J. Pienta, C. Abate-Shen, D. B. Agus, R. M. Attar, L. W. Chung, N. M. Greenberg, W. C. Hahn, J. T. Isaacs, N. M. Navone, D. M. Peehl, J. W. Simons, D. B. Solit, H. R. Soule, T. A. VanDyke, M. J. Weber, L. Wu, R. L. Vessella, "The current state of preclinical prostate cancer animal models," *Prostate* **68**(6), 629−639 (2008).